N73-10142

38. Human Operator Dynamics for Aural Compensatory Tracking*

EDWARD W. VINJE

United Aircraft Research Laboratories

AND

EDWARD T. PITKIN

University of Connecticut

The human operator's ability to control using aural information only and using combined aural and visual displays was investigated for a simple tracking task. Tracking error was presented to the test subjects using one- and two-ear displays. For both displays the pitch of the tone represented the magnitude of the tracking error. **Error** polarity was indicated in the two-ear display by switching the tone between ears as a function of error sign. **For** the one-ear display, error polarity was indicated by using modulated and unmodulated tones.

The operator's aural control characteristics were modeled as a describing function plus a remnant. The effects on the measured describing function and remnant of different system dynamics, changes in the frequency content of the input and different displays were determined during the study.

The describing function and remnant data indicate that humans can control as well with aural cues as with visual cues for the task considered. However, the reduction in operator time delays, expected because of the generally faster human response to aural stimuli, was not evident in the results. It was also determined that the operators could control equally well with either the one- or two-ear display. Differences which might exist between monaural and binaural signal processing in the human operator were not significant for the displays and task considered. Finally, the operator model results indicate that the combined aural and visual presentation of tracking error neither improves the operator's control capability nor reduces operator time delays. Reduced time delays might have been expected because studies of simple human response have shown faster response to combined aural-visual stimuli, then to either stimulus alone.

INTRODUCTION

There are a number of aircraft control tasks in in which excessive demands are placed on the pilot's capability to control visually. Examples of such tasks are terrain following and V/STOL aircraft IFR approach and hover. Integrated and heads-up displays have been developed in an attempt to reduce the visual workload for such tasks. However, supplying the pilot with control information through one or more of his other sensory channels could also alleviate visual workload. In addition, using these other senses might enable the pilot to be more flexible with his vision than he could be with visual displays alone.

The human's aural sense is an information collecting apparatus which might be used as an alternate to vision in complex control tasks. In some respects, the aural channel may actually be superior to vision as an information gathering and processing device for human control. For example, the human aural receptor delays are considered to be smaller than the visual receptor

*This research was performed at the University of Connecticut to fulfill part of the requirements for E. W. Vinje's Ph.D degree.

latencies (ref. **1).** Also, studies of simple human response indicate that an aural stimulus elicits a response which may be **10** to **30** msec faster than the response to a visual stimulus (refs. **1** and **2).** Thus, it may be that the pure time delays incurred in aural control would be smaller than those for visual control.

Little attention has been given to the human operator's ability to control using aural information in previous man-machine system studies. This study was undertaken, therefore, to quantitatively evaluate the human operator's aural control characteristics. The limits of the human's aural control capability and also his flexibility as an aural controller were considered in the investigation. The effects of combined aural and visual presentation of control information were also examined. Particular emphasis was placed on obtaining results which would permit a quantitative comparison of human aural and aural-plus-visual control characteristics with results for control with visual information only.

MODEL FOR THE HUMAN OPERATOR

The test subject's dynamic characteristics for aural control were modeled as a describing function $Y_p(j\omega)$ plus a remnant $\phi_{nn}(\omega)$ which was assumed to be injected at the subject's output. This model is shown in figure 1. The describing function defines the linear relation between tracking error and operator output at the frequencies contained in the task input $i(t)$. As such, it can be used to define that part of the pilot's output which is linearly correlated with the input. The remnant, in turn, is composed of that part of the operator's output which is not linearly correlated with the input. The describing function and remnant measured in this study were developed from the functions $e(t)$ and $c(t)$ which were recorded during 180-sec tracking periods. These functions were digitized off-line and Fourier coefficients were computed from these data at appropriate frequencies using a fast Fourier transform algorithm. The Fourier coefficients were then used to form the describing function and remnant.

The mean-square value of the operator's output $c^2(t)$ was also measured during the tracking runs. These data were used in conjunction with

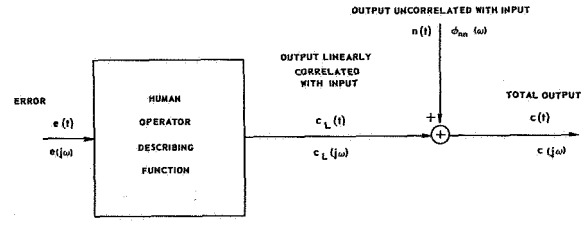

FIGURE 1.—Model for human operator dynamics.

the task input $i(t)$ and the operator's describing function to form operator relative remnant ρ_a^2. Relative remnant is defined as the ratio of the mean-square value of that part of the operator's output linearly correlated with the input $c_L^2(t)$ to the mean-square value of the total operator output $\overline{c^2(t)}$. That is,

$$\rho_a^2 = \frac{\overline{c_L^2(t)}}{\overline{c^2(t)}} = \frac{\overline{c^2(t)} - \overline{n^2(t)}}{\overline{c^2(t)}} \tag{1}$$

where $\overline{n^2(t)}$ is the mean-square value of operator remnant. Relative remnant is, therefore, an indication of relative operator linearity.

Describing functions measured in this study were also fit visually with two linear models. The first representation, McRuer's crossover model, was fit to forward-loop describing functions developed by forming the product $Y_p(j\omega) \cdot Y_c(j\omega)$, where $Y_c(j\omega)$ is the transfer function for the controlled element. The crossover model is defined as

$$Y_p(j\omega) \cdot Y_c(j\omega) \approx \frac{\omega_c e^{-j\omega\tau_e}}{j\omega} \tag{2}$$

where ω_c is the crossover frequency and τ_e is an approximation for the effects of operator lags and delays and high-frequency lead generation. In order for the crossover model to be a valid representation for $Y_p(j\omega) \cdot (Y_c(j\omega)$, the operator must compensate the controlled element dynamics so as to achieve a $K/j\omega$ forward-loop describing function at frequencies near crossover. Such a forward-loop describing function is indicative of "good" closed-loop response (ref. **3).**

The second model used to represent selected operator describing functions, $Y_p(j\omega)$, measured in this study was a more complex transfer function. This representation is McRuer's precision model which is defined as

$$Y_p(j\omega) \approx G\left(\frac{T_K j\omega+1}{T_{KI} j\omega+1}\right)\left(\frac{T_L j\omega+1}{T_I j\omega+1}\right)\frac{e^{-j\omega\tau}}{(T_{N1} j\omega+1)[(T_{N2} j\omega)^2+T_{N3} j\omega+1]} \quad (3)$$

where

G = adaptable operator gain

$\frac{T_K j\omega+1}{T_{KI} j\omega+1}$ = low frequency lag-lead form presumed to describe low-frequency effects of the neuromuscular system dynamics

$(T_L j\omega+1)$ = adaptable lead compensation

$(T_I j\omega+1)$ = adaptable lag compensation

$e^{-j\omega\tau}$ = pure time delay due to latencies in the aural data gathering, coding and transmission process

$\frac{1}{(T_{N1} j\omega+1)[(T_{N2} j\omega)^2+T_{N3} j\omega+1]}$ = representation for the high-frequency characteristics of the neuromuscular system dynamics.

The precision model was found to be a reasonably accurate representation over all measurement frequencies for the visual describing functions measured in reference **3.** Note also that the precision model identifies separate operator dynamic characteristics whose effects had been combined in the crossover model for $Y_p(j\omega)\cdot Y_c(j\omega)$, e.g., the pure time delay and the high-frequency effects of the neuromuscular dynamics.

DESCRIPTION OF THE AURAL CONTROL EXPERIMENT

Control Task, Aural Displays and Manipulator

The control task considered in this study was one-degree-of-freedom compensatory tracking. A schematic of the task is shown in figure **2.** Important features of the task are discussed briefly in the following paragraphs. A more detailed description can be found in reference **4.** The input $i(t)$ which the test subjects tracked was McRuer's "sum-of-sine waves" function (ref. **3).** The bandwidth of this function was varied during the investigation to change the difficulty **of** the task. For aural control the tracking error voltage $e(t)$ was converted to an audio signal and presented using two-ear and one-ear displays. Both two- and one-ear displays were considered in order to provide information on display requirements for the human aural controller.

For both aural displays $e(t)$ was linearly converted to frequency and the magnitude of the tracking error was represented by the pitch of a single tone. The sensitivity used in converting tracking error voltage to frequency was **64** Hz/volt. This was the sensitivity which resulted in the best aggregate tracking performance from the test subjects used in this study. Zero tracking error corresponded to a low-frequency **(330** Hz) bias tone. For the two-ear display, the sign of the tracking error was indicated by switching the tone between the left and right earphones. The convention on the switching was such that the control stick was moved away from the ear in which the tone was heard. This in turn reduced the magnitude of the tracking error and the perceived pitch of the tone. For example, if the tone was heard in the left ear and the stick was moved right, the pitch of the tone decreased until it reached the bias frequency of **330** Hz. At this point the tone would switch to the right ear and begin to increase in pitch,

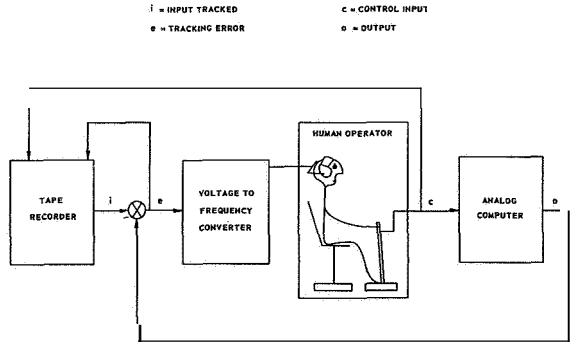

FIGURE 2.—Schematic diagram of the aural compensatory tracking experiment.

indicating that the sign of $e(t)$ had changed and that its magnitude was becoming larger.

The frequency to voltage sensitivity and the bias frequency used for the one-ear display were the same as those for the two-ear display. The only difference between displays was in the manner in which the polarity of $e(t)$ was presented. For the one-ear display, a change in the sign of the error was indicated by changing the character of the presented tone. A negative tracking error resulted in a tone identical to that used in the two-ear display. For positive tracking error the tone was modulated, i.e., for positive error the tone seemed to "whir" as it changed pitch.

The control stick used was a cantilevered rectangular steel rod which provided a stick force gradient of 1.0 lb/in. The top of the stick could be moved ± 3 in. about null before it contacted stops. Motion of the stick was converted to the voltage $c(t)$ using a linear induction transducer. The sensitivity of the control stick was held constant and the forward-loop gain of the system was adjusted to acceptable values by changing the gain of the controlled elements. The controlled element dynamics were simulated using an analog computer as shown in figure 2.

Test Cases and Subjects

The test cases for which describing functions, remnants and relative remnants were measured are shown in table 1. The major part of this study consisted of a relatively complete evaluation of aural human operator dynamics using both the one-ear and two-ear displays. The remainder of the study consisted of a short investigation of the effects on operator dynamics of combined aural and visual presentation of tracking error. Data were obtained from three test subjects for each of the test cases indicated in table 1. All subjects had normal hearing, but none had any special talent for identifying the characteristics of audio tones, e.g., perfect pitch. Also, one of the subjects was an experienced visual tracker, but none had any previous aural tracking experience.

DESCRIBING FUNCTION RESULTS

Results for the Two-Ear Display

Describing functions.—Representative forward-loop describing functions $Y_p(j\omega) \cdot Y_c(j\omega)$ for the two-ear display are shown in figures 3, 4, and 5 for $\omega_b = 2.6$ rad/sec and controlled elements of 10, $10/j\omega$ and $10/(j\omega)^2$, respectively. The standard deviations in these measurements are presented as well. Visual describing functions from reference 3 for corresponding controlled elements and a similar input ($\omega_b = 2.5$ rad/sec) are also plotted for comparison in figures 3, 4, and 5. In addition, the crossover model has been fit to the aural data and is plotted in these figures. The discussion of these describing function results which follows for $\omega_b = 2.6$ rad/sec applies also to similar data obtained with $\omega_b = 1.7$ and 3.5 rad/sec (ref. 4). The aural results presented in figures 3, 4, and 5 indicate that the test subjects adapted to the controlled elements so as to yield describing function magnitudes similar to those of a $K/j\omega$ transfer function. This is especially evident for the $10/j\omega$ and $10/(j\omega)^2$ controlled elements where the crossover model fits the describing function magnitude quite well. Note also, that the magnitudes (and crossover frequencies) of the aural describ-

TABLE 1.—Test Cases Evaluated

Investigation	Display	Controlled element	Input break frequency, ω_b-rad/sec
Aural presentation of tracking error	Two ear	K, $K/j\omega$, $K/(j\omega)^2$	1.7, 2.6, 3.5
	One-ear display on left ear	$K/(j\omega)^2$	1.7, 2.6
	One-ear display on right ear	$K/(j\omega)^2$	1.7
Combined aural and visual presentation of tracking error	Visual only	$K/(j\omega)^2$	2.6
	Two-ear aural	$K/(j\omega)^2$	2.6
	Visual plus two-ear aural	$K/(j\omega)^2$	2.6

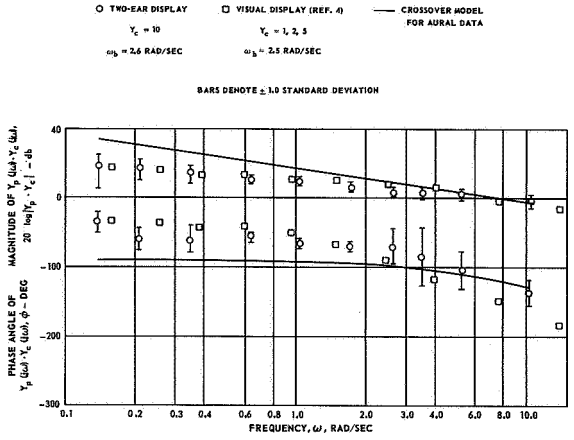

FIGURE 3.—Comparison of aural and visual forward-loop describing functions for gain dynamics.

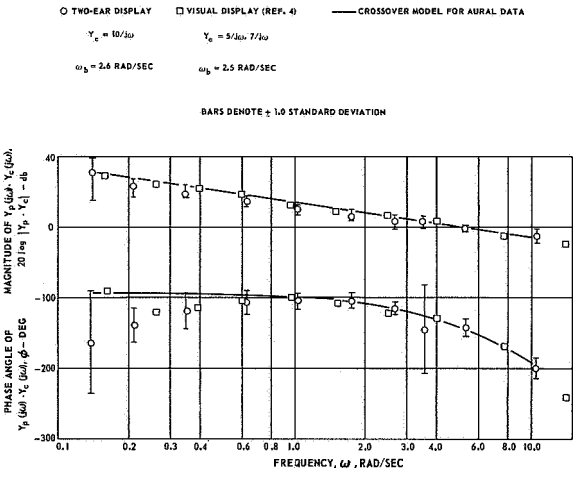

FIGURE 4.—Comparison of aural and visual forward-loop describing functions for rate dynamics.

ing functions generally decreased with increasing order of the controlled element. The effect of ω_b on the aural describing function characteristics will be discussed later in conjunction with the crossover model parameters.

The visual describing function data from reference **3** generally agree well with the corresponding aural results. The magnitudes correspond closely for all controlled elements and the phase angles are also very similar for the $10/j\omega$ and $10/(j\omega)^2$ controlled elements. However, for the gain controlled element the phase lag of the aural data is generally smaller at the higher

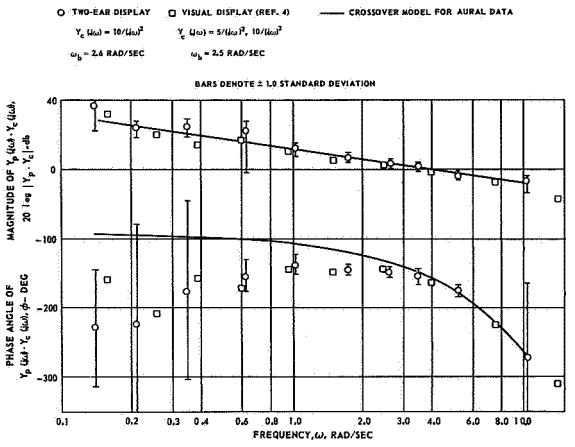

FIGURE 5.—Comparison of aural and visual forward-loop describing functions for acceleration dynamics.

frequencies than the phase lag for the visual results.

Crossover model parameters.—*As* indicated previously, the crossover model accurately represents the magnitude of the aural forward-loop describing functions for the $10/j\omega$ and $10/(j\omega)^2$ controlled elements. However, only for frequencies near crossover is this model a good representation of the magnitude of the describing function for the gain controlled element (see figs. **3, 4,** and 5). For all controlled elements, the model does not represent the describing function phase angles accurately for frequencies much below crossover. These conclusions apply to aural describing functions obtained for all three values of ω_b (ref. **4).**

The crossover model parameters used to fit the aural describing functions for all values of ω_b are listed in table **2.** Phase margins associated with these fits are also presented along with visual describing function parameters computed from empirical formulas developed in reference **3.** It should also be pointed out that the gains of the controlled elements were increased for aural tracking when ω_b was increased. The test subjects desired increased forward-loop gain when ω_b was made larger and the input became more difficult to track. The controlled element gains were not adjusted in this fashion for the visual study of reference **3.**

The relative magnitudes of corresponding aural and visual crossover model parameters are

TABLE 2.—*Comparison* of Aural and Visual *Crossover* Model Parameters

ω_b, rad/sec	Dynamics	Aural, two-ear display			Visual, ref. 3		
		ω_c, rad/sec	PM, deg	τ_e, sec	ω_c, rad/sec	PM, deg	τ_e, sec
1.7	7	5.2	73	0.06	5.1	35	0.19
	$7/j\omega$	4.6	48	0.16	4.7	31	0.22
	$7(j\omega)^2$	3.7	20	0.32	3.3	18	0.38
2.6	10	6.8	63	0.06	5.2	54	0.12
	$10/j\omega$	4.8	41	0.18	4.8	48	0.15
	$10/(j\omega)^2$	3.9	23	0.30	3.5	28	0.31
3.5	15	4.8	78	0.05	5.4	75	0.05
	$15/j\omega$	4.2	54	0.14	5.0	67	0.08
	$15/(j\omega)^2$	3.8	27	0.30	3.7	40	0.24

similar and the trends in the aural and visual parameters with controlled element order are the same. That is, ω_c and PM decrease and τ_e increases with increasing controlled element order for both sets of data. However, there are trends in the visual data with ω_b which are not evident in the aural results. Crossover frequency and phase margin increase and τ_e decreases with ω_b for the visual data and these trends are not evident in the aural results. The aural ω_c does increase slightly as ω_b changes from *1.7* to *2.6* rad/sec, however. Note also that operator regression * is not apparent at $\omega_b = 3.5$ rad/sec in the aural results for the $K/(j\omega)^2$ controlled element. Regression is not evident in the visual data of reference *3* either since the formulas used to fit the data do not account for its effects. However, other visual results in reference *3* show that the operators regressed significantly at $\omega_b = 4.0$ rad/sec with the $K/(j\omega)^2$ controlled element ($\omega_c = 1.8$ rad/sec and PM = 42° at $\omega_b = 4.0$ rad/sec versus $\omega_c = 3.25$ rad/sec and PM = 26° at $\omega_b = 2.5$ rad/sec).

Both the crossover model parameters and the describing functions themselves tend to indicate little difference between human operator dynamics for aural and visual control. In particular, a smaller time delay, which might have been expected for the aural results because of the smaller aural receptor latency, were not evident in the crossover model results. That is, the aural values of τ_e were not significantly smaller than the visual τ_e results.

Precision model parameters.—The precision model (eq. *(3)*) was fit to all the two-ear display describing function data and these results are presented in reference *4*. Two interesting features of these data will be discussed here. First, the values of operator adapted lead used to fit the aural describing function data for the $K/(j\omega)^2$ controlled elements were equivalent to the lead adapted by the subjects in the visual tracking study of reference **3.** The aural lead parameters are presented in the following list:

ω_b	$Y_c(j\omega)$	T_L
1.7	$7/(j\omega)^2$	*3.7*
2.6	$10/(j\omega)^2$	*3.7*
3.5	$15/(j\omega)^2$	*3.0*

Secondly, visual data are available (ref. **3)** which permit a reasonably direct comparison between aural and visual precision model parameters. The aural data are for the $10/j\omega$ controlled element with $\omega_b = 2.6$ rad/sec. The visual parameters are for $Y_c(j\omega) = K/(j\omega - 2)$ and $\omega_b = 2.5$ rad/sec. How well the precision model fits the aural data can be seen in figure **6.** The visual and aural precision model parameters are tabulated in the following list:

	T_L	T_I	T_K	T_{KI}
Visual	*0.11*	0.0	*3.33*	*20.0*
Aural	*0.05*	0.0	*5.50*	*25.0*

* **Regression is a term used to describe the relaxation in operator control characteristics (decreased ω_c and increased PM) which occurs when the tracking task is made too difficult.** In **doing so the operator tolerates a larger tracking error in the interest of maintaining stability.**

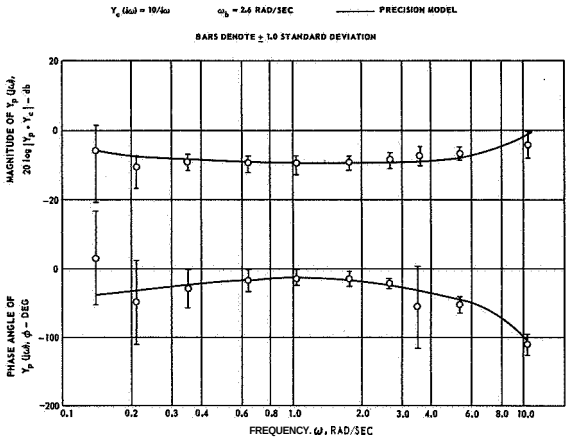

FIGURE 6.—Precision model fit to operator describing function for rate dynamics with two-ear display.

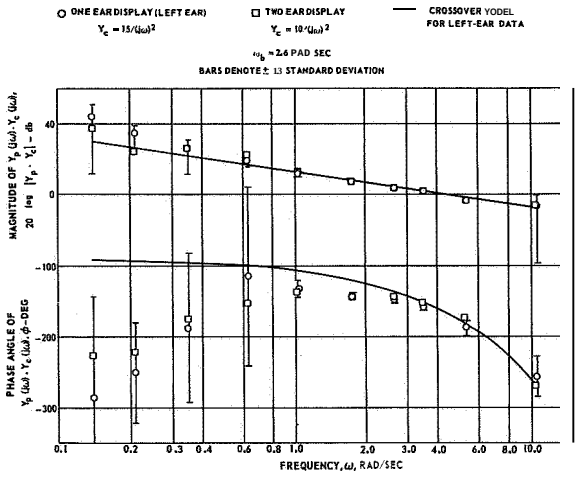

FIGURE 7.—Forward-loop describing functions for acceleration dynamics with one- and two-ear displays.

	τ	T_{N1}	T_{N2}	T_{N3}
Visual	**0.09**	**0.10**	**0.06**	**0.014**
Aural	**0.10**	**0.08**	0.08	**0.016**

The visual and aural parameters are very similar. Note that the pure time delay parameter τ is not smaller for the aural data.

Results for the One-Ear Display

A representative forward-loop describing function for the one-ear display is shown in figure 7. It was measured for $\omega_b = 2.6$ rad/sec and $Y_c(j\omega) = 15/(j\omega)^2$ with the display on the left ear. The crossover model fit to this data is also shown in figure 7. For comparison, a describing function for the two-ear display measured with the same input break frequency and $Y_c(j\omega) = 10/(j\omega)^2$ is presented as well. The controlled element gains used with the one-ear display were larger than those considered for the two-ear display. The test subjects felt the larger gains compensated somewhat for the less precise indication of tracking error sign change in the one-ear display. As indicated in figure 7, the one-ear display and two-ear display describing functions are quite similar. This correspondence between one-ear and two-ear display describing functions holds for the other one-ear display test cases considered as well, i.e., $\omega_b = 1.7$ rad/sec, and $Y_c = 10/(j\omega)^2$ with the display on either the right or left ear. Crossover model parameters obtained for these comparative one-ear and two-ear display test cases are discussed in reference 4. There appears to be no significant difference between the one-ear (used on either the right or left ear) and two-ear display crossover model parameters.

Results for Combined Aural and Visual Displays

Description of visual display.—As indicated in table 1, describing functions were measured in this part of the study using an aural display only, a visual display only and the aural and visual displays in combination. The aural display used was the two-ear display described previously. Initially, a scaled oscilloscope face with a grid and a zero-error reference was considered for use as the visual display. However, experiments indicated that this display provided more precise information than the aural display. The subjects ignored the aural display when it was used in combination with the scaled visual display. This could have compromised the objectives of this part of the study.

The visual display that was finally used was an oscilloscope display designed to be a visual analog of the two-ear aural display. It is shown schematically in figure 8. On this display a dot moved along one of two separate vertical paths. One of the paths was located on the left side of

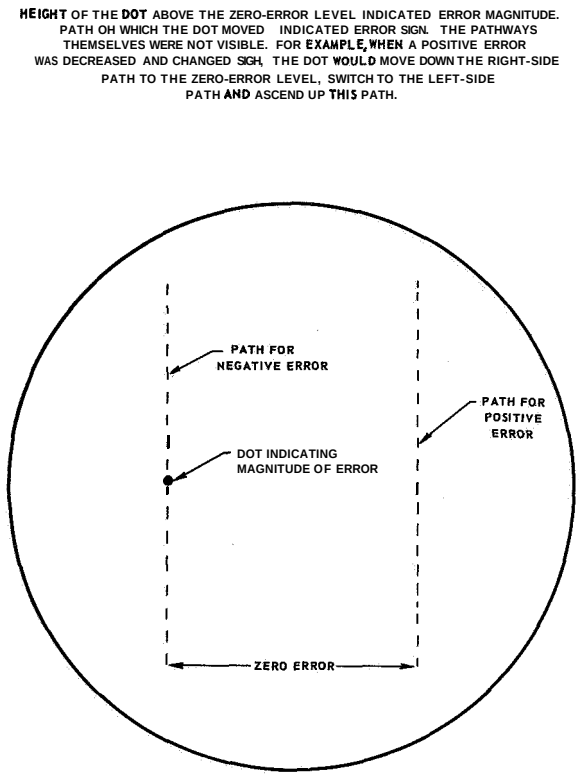

FIGURE 8.—Oscilloscope display used in the evaluation of combined aural and visual displays for tracking error.

the oscilloscope face and the other was located on the right. The magnitude of the tracking error was indicated by the vertical position of the dot and the sign of the error determined which path the dot moved on. The oscilloscope face did not have a scaled grid and there was no reference line for zero error. Measured rms tracking errors for this display were only slightly larger than corresponding tracking error scores measured for the aural two-ear display. It was felt, therefore, that the visual display provided about as much information on tracking error as did the two-ear display.

Describing functions.—Describing functions measured for aural only, visual only and combined (or parallel) aural and visual displays are presented in figure 9. These describing functions were measured for $10/(j\omega)^2$ dynamics and $\omega_b = 2.6$ rad/sec. The one standard-deviation error bars are shown for the combined display data and the crossover model fit to the combined display data is also shown. The describing functions for all

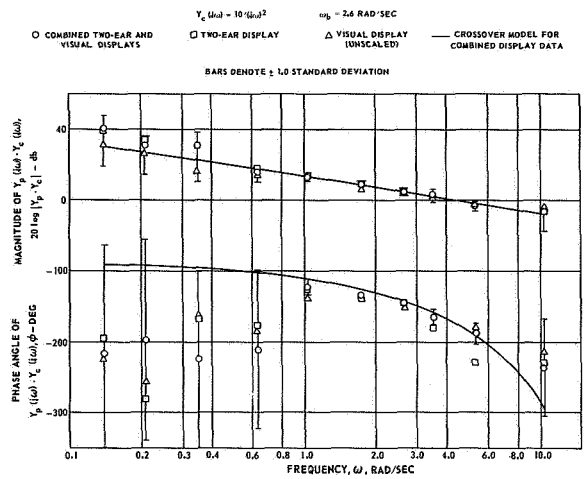

FIGURE 9.—Forward-loop describing functions for acceleration dynamics with aural, visual, and combined displays.

three types of tracking error presentations are generally quite similar.

Crossover model parameters.—Parameters used to fit the crossover model to the three describing functions shown in figure 9 are listed in table 3. The crossover frequency is slightly larger and the phase margin smaller for the combined displays than for either display alone. Although the ω_c and PM differences are small, they do indicate that the operators were slightly more responsive to tracking error when the displays were combined. This correlates with the slightly smaller rms tracking error scores measured for the combined displays (ref. 4). The value of τ_e, however, was no smaller for the combined displays. As was pointed out previously, studies of simple human response (ref. 1) have shown that humans respond more rapidly to combined aural and visual stimuli than to an aural stimulus alone. Studies also indicate, however, that the latency in human response is related to the complexity of the required response (ref. 1). The compensatory tracking task may be sufficiently difficult to obscure differences which are significant for more simple human response tasks.

REMNANT RESULTS

Remnant power spectral densities $\phi_{nn}(\omega)$ measured for the unscaled visual display and the

TABLE 3.—*Crossover Model Parameters for Aural, Visual and Combined Displays*
[$\omega_b = 2.6$ rad/sec, $Y_c/(j\omega) = 10/(j\omega)^2$]

Display	Crossover model parameters		
	ω_c, rad/sec	PM, deg	τ_e, sec
Aural (two-ear)	3.9	18	0.34
Visual	3.8	23	0.30
Combined aural and visual	4.2	8	0.34

two-ear aural display are compared in figure 10. The remnant power spectral density for the scaled visual display mentioned previously is also presented in figure 10. These data were measured for $\omega_b = 2.6$ rad/sec and $Y_c(j\omega) = 10/(j\omega)^2$ and the results are presented in terms of power decibels (pdb) where $\text{pdb}(\omega) = 10\log_{10}\phi_{nn}(\omega)$. It should be noted, also, that the effects of measurement and computational errors become significant in the remnant data for frequencies below 0.6 rad/sec (ref. **4**). Therefore, the remnant data are not reliable at these low frequencies. However, for frequencies equal to or greater than 0.6 rad/sec, the visual and aural remnant data agree quite well. The averaged relative remnant results, ρ_a^2, for these test cases are quite small, however, they also are quite similar. These values of ρ_a^2 are 0.06, 0.06, and 0.07 for the aural, unscaled visual, and scaled visual displays, respectively.

Remnant data from this study are discussed in more detail in reference **4.** Some of the more significant results from the analyses of these data will be briefly outlined here. The remnant power spectral data in reference **4** show that the magnitude of the remnant spectra increased with increasing order of the controlled element. The values of relative remnant, ρ_a^2, varied inversely with controlled element order, ranging in magnitude from about 0.90 for $Y_c = K$ to 0.10 for $Y_c = K/(j\omega)^2$ at $\omega_b = 2.6$ rad/sec. The remnant power spectral magnitudes for a given controlled element decreased with increasing ω_b. This was due chiefly to the increased controlled element gain used as ω_b was made larger. The increased gain resulted in smaller control motions which resulted in lower remnant power spectral densities and also smaller total operator control

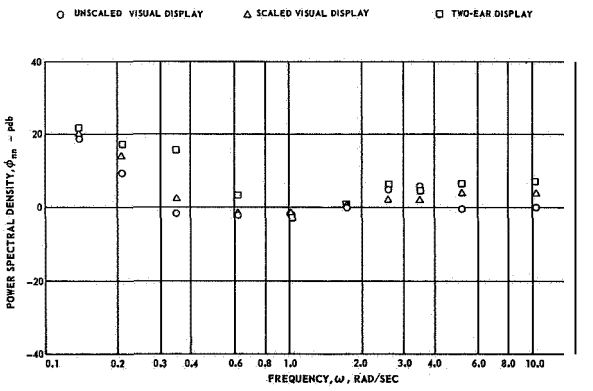

FIGURE 10.—Remnant power spectra for acceleration dynamics with unscaled visual, scaled visual, and aural displays.

output. The averaged values of ρ_a^2 generally decreased when ω_b was increased. Also, the remnant power spectral densities and relative remnant results for the two-ear and one-ear aural displays were not significantly different.

SYMBOLS

c	total operator output, volts
$\overline{c^2}$	mean-square total operator output, (volts)^2
$\overline{c_L^2}$	mean-square value of that part of the total operator output linearly correlated with the input, (volts)^2
db	decibels, $20\log_{10}(\ )$ where $(\ )$ is a magnitude quantity, e.g., Y_p
e	tracking error, volts
G	gain of the precision model, volts/volt
i	input forcing function, volts
j	$\sqrt{-1}$
K	open-loop gain, volts/volt
n	operator open-loop remnant injected at the operator's output, volts
$\overline{n^2}$	mean-square operator open-loop remnant, (volts)^2
0	output from the controlled element, volts
pdb	power decibels, $10\log_{10}(\ )$ where $(\ )$ is the quare of a magnitude quantity, e.g., ϕ_{nn}
PM	phase margin, an indicator of closed-loop stability expressed as the phase lag of the forward-loop describing function, ϕ, plus 180°, deg
s	Laplace operator, 1/sec

T_I time constant for operator adapted lag, sec

T_K lead time constant for the lead-lag representation of operator low-frequency neuromuscular characteristics, sec

T_{KI} lag time constant for the lead-lag representation of operator low-frequency neuromuscular characteristics, sec

T_L time constant **for** operator adapted lead, 0ec

T_{N1} time constant for first-order lag portion of the third-order precision model representation for operator high-frequency neuromuscular characteristics, sec

T_{N2} coefficient in the second-order part of the precision model representation for operator high-frequency neuromuscular characteristics, sec^2

T_{N3} coefficient in the second-order part of the precision model representation for operator high-frequency neuromuscular characteristics, sec

Y_c controlled element transfer function

Y_p measured operator describing function

ρ_a^2 operator relative remnant (see eq. **(1))**

τ time constant representing inherent operator time delays, sec

τ_e time constant approximating the effects of operator time delays, neuromuscular lags and high-frequency operator adapted lead, sec

ϕ phase angle of the forward-loop describing function, $Y_p \cdot Y_c$, deg

ϕ_{nn} power spectrum **of** the open-loop remnant injected at the operator output, $(volts)^2/rad/sec$

ω frequency, rad/sec

ω_b bandwidth of the input to the tracking task, rad/sec

ω_c crossover frequency, that frequency at which the gain of the forward-loop describing function, $Y_p \cdot Y_c$, is equal to one; a measure of closed-loop frequency response, rad/sec

REFERENCES

1. WARGO, M. J.; ET AL.: Human Operator Response Speed, Frequency, and Flexibility: **A** Review, Analysis and Device Demonstration. NASA CR–874, Sept. 1967.
2. SINAIKO, H. W., ED.: Selected Papers on Human Factors in the Design and Use of Control Systems. Dover Publications (New York), 1961.
3. MCRUER, D. T.; GRAHAM, D.; KRENDELL, E. S.; **AND** REISENER, W. : Human Pilot Dynamics in Compensatory Systems. AFFDL–TR–65–15, July 1965.
4. VINJE, E. W.: Human Operator Dynamics for Audio Compensatory Tracking. Ph.D Thesis, Department of Aerospace Engineering, Univ. of Connecticut (in preparation).